Beyond the Reverse Horiuti-Polanyi Mechanism in Propane Dehydrogenation over Pt Catalysts

Ling Xiao,[†,#] Yu-Ling Shan,[†,#] Zhi-Jun Sui,[†] De Chen,[‡] Xing-Gui Zhou,[†] Wei-Kang Yuan,[†] Yi-An Zhu[†,*]

[†]UNILAB, State Key Laboratory of Chemical Engineering, School of Chemical Engineering, East China University of Science and Technology, Shanghai 200237, China

[‡]Department of Chemical Engineering, Norwegian University of Science and Technology, N-7491 Trondheim, Norway

KEYWORDS: Dehydrogenation mechanism, Platinum, Microkinetic analysis, DFT, Adsorbate-adsorbate interactions

ABSTRACT: Catalytic dehydrogenation of light alkanes over Pt catalysts is generally accepted to follow a reverse Horiuti-Polanyi mechanism. By using microkinetic analysis in combination with results from density functional theory calculations, we show that, although propane dehydrogenation (PDH) occurs by two successive dehydrogenation steps on terraces, an unexpected non-reverse Horiuti-Polanyi mechanism accounts for more than half the propylene production at the under-coordinated active sites that dominate the kinetics of PDH. The main reaction is composed of three dehydrogenation steps that have two β-H and one α-H atoms removed from propane, followed by the hydrogenation of CH_3CCH_2, and, starting from this species, the formation of propylene and by-products proceeds by way of two parallel competing reactions. The proposed mechanism has been verified by exploring several key and general aspects of the kinetic behavior observed in the dehydrogenation of light alkanes, and it is found that, only when adsorbate-adsorbate interactions are taken into consideration can the experimentally determined kinetics be properly reproduced. Increasing the H_2 partial pressure from low values favors an increase in the coverage of free sites due to gasification of adsorbed coke precursors, which in turn gives rise to lowered energy barriers for C-H bond breaking, thereby achieving an increased propane consumption rate. As the H_2/C_3H_8 ratio rises, the rate for propylene production first goes up and then declines and a maximum is observed at a H_2/C_3H_8 ratio of 1.33, which occurs when the negative effect of the increased free fourfold hollow sites bringing about deep dehydrogenation begins to dominate the positive effect of the increased free step sites that are responsible for activating propane. The mechanism formulated here proves to be valid even if temperature, pressure, or the H_2/C_3H_8 ratio is varied, and hence provides a foundation for rational design of metal and alloy catalysts for light alkane dehydrogenation.

1. INTRODUCTION

Propylene, which is an important chemical intermediate in the petrochemical industry, has conventionally been produced either as a co-product to ethylene in steam crackers or as a byproduct in refineries.[1-2] Since the start of this century, the shale gas revolution in North America has made a significant impact on the global energy market. In addition to methane, shale gas deposits contain a considerable amount of ethane and propane.[3-4] As a consequence, new steam cracker projects are based primarily on ethane as feedstock and can only produce a negligible amount of propylene, which gives rise to an increased propylene supply-demand gap. On the other hand, the shale-based propane is relatively cheap, making the current market conditions very favorable for propylene production via dehydrogenation.[5] For this reason, the propylene supply chain has been moving away from co-production and towards on-purpose production.

The catalytic dehydrogenation of propane is a reversible reaction where the equilibrium position lies too far to the reactant side and the propylene yield is severely limited by thermodynamics. Because of its highly endothermic character under standard conditions at 298 K ($\Delta_r H^\circ$ = 123.8 kJ/mol), the operating temperature of the existing commercial processes is typically kept as high as 800 ~ 980 K to achieve a reasonable propane conversion.[6] The increase in temperature, however, has a negative effect on the catalyst selectivity because side reactions, such as cracking, hydrogenolysis, deep dehydrogenation, oligomerization, cyclization, and coke formation, are

promoted even more dramatically at high temperatures.[7-8] As a result, despite the simplicity in appearance of the main reaction, the undesirable side reactions constitute a huge reaction network and yield a wide variety of C1 to C3 intermediates adsorbed on the catalyst surface, making the reaction mechanism enormously complex.[9-10]

The first step in the kinetic analysis of reactions is to establish the stoichiometry and network of the reaction. Inclusion of all possible elementary steps is essential to an accurate description of the kinetics. In most of previous theoretical and experimental studies, propane dehydrogenation (PDH) is thought of as occurring by the reverse Horiuti-Polanyi mechanism,[1, 11-16] involving only two successive dehydrogenation steps in the propane molecule, followed by desorption of propylene and H_2 from the catalyst surface. In this way, the reaction pathway is actually *a priori* specified and, more importantly, without allowing the formation of undesired products such as methane and ethylene, one cannot determine the selectivity toward propylene by means of calculation and simulation. In PDH, whether propylene would be released from the catalyst surface or undergo deep dehydrogenation is of central importance because it not only determines the yield of propylene but is intimately related to the amount of coke deposited, and hence to the catalyst stability. Although we have pointed out in an early study that the activation energy difference between propylene dehydrogenation and desorption provides a measure of the catalyst selectivity[17], which has now been widely used as a descriptor to screen promising candidates as the catalyst for PDH[12-13, 18-19], the application of such a simple energetic quantity is apparently inadequate for more quantitative discussions.

Theoretically, the only two kinetic studies that take the side reactions into consideration so far are concerned with the mechanism of PDH over the flat Pt(111) surface,[20-21] which is based on the idea that the under-coordinated sites would be preferentially blocked due to coke formation.[12, 22-25] On the other hand, it remains an open question whether the unsaturated Pt sites are deactivated permanently and completely throughout the dehydrogenation reaction. First, it was suggested by in-situ and ex-situ HRTEM and TAP that coke formed on the active metal surface can be moved to the catalyst support[24, 26] and the ability of the support to accommodate coke often determines the catalyst stability. Second, the kinetics of the dehydrogenation reaction was found to be strongly size-dependent.[12, 27] Even after the reaction has reached a steady-state, small Pt clusters can still give a much higher turnover frequency (TOF) than large ones, which means that the under-coordinated sites that dominate the surface of small clusters must play a role in catalyzing the reaction. Third, the recently discovered single-atom catalysts and pseudo-single-atom catalysts exhibit superior catalytic performance in a wide variety of chemical reactions, both of which have a high density of under-coordinated metal atoms and are believed to be highly active for PDH.[28-30] Hence, the complex reaction mechanism, even on the most widely studied Pt catalyst, has not yet been fully elucidated and a full picture of how the reaction proceeds can only be achieved through an understanding of the way in which various active sites behave and contribute to the overall kinetics.

In addition, much of our present understanding of the kinetics of heterogeneous reactions is based on the Langmuir isotherm, which assumes the independence and equivalence of adsorption sites. Deviation from the isotherm can be traced to the failure of these assumptions. For example, the enthalpy of adsorption depends on the extent of surface coverage, mainly because the adsorbed species interact. If the species repel each other (as in most cases) the adsorption becomes less exothermic (the enthalpy of adsorption becomes less negative) as coverage increases.[31-33] Because the interactions between adsorbates may affect the energetics of elementary steps in different ways and to different extents, the reaction mechanism could be markedly different with and without considering this effect.

In this work, we have performed a combined experimental and theoretical study to formulate the catalytic reaction mechanism for PDH over both the close-packed Pt(111) and the stepped Pt(211) surfaces. The kinetics of PDH, specifically the effect of the H_2/C_3H_8 ratio on the catalytic activity and propylene selectivity, is first examined experimentally, and the central feature of this kinetic analysis is considered to validate the theoretically determined kinetics. Then, a detailed density functional theory (DFT)-assisted microkinetic model is built under the steady-state approximation and with adsorbate-adsorbate interactions considered. Next, the active site, the dominant reaction pathway, and the key factors determining the catalyst activity and propylene selectivity are revealed. Finally, we conclude by discussing the implication of our results for understanding the non-reverse Horiuti-Polanyi mechanism for the dehydrogenation of light alkanes.

2. METHODS

2.1. DFT Calculation

DFT calculations were performed with the VASP[34-36] package using plane wave basis sets. A plane wave energy cutoff of 400 eV was used in the calculations to achieve a tight convergence. The interactions between valence electrons and ion cores were represented by Blöchl's all-electron-like projector augmented wave (PAW) method.[37] Brillouin zone sampling was performed by using a Monkhorst-Pack grid[38] with respect to the symmetry of the system. The electronic occupancies

were determined according to a Methfessel-Paxton scheme[39] with an energy smearing of 0.2 eV. The description of van der Waals forces is important for the C2 and C3 species involved in PDH,[13, 20] so the exchange and correlation in the Kohn-Sham theory were treated with the BEEF-vdW functional.[40] In a previous study, Gautier et al.[41] showed that, compared with other vdW functionals, the BEEF-vdW functional makes reasonably reliable predictions of the geometries and energetics of the adsorption of covalently bound molecules such as ethylidyne on Pt(111).

A five-layer slab with a *p*(3 × 3) supercell was used to represent the Pt(111) surface. The neighboring slabs were separated by a vacuum region as thick as 12 Å to eliminate the periodic interactions in the direction perpendicular to the surface. The bottom two layers were fixed to their crystal lattice positions, while all the other atoms were allowed to fully relax. When studying the reactions on Pt(211), a *p*(1 × 3) supercell with fifteen layers was used, and the bottom six layers were fixed. The Monkhorst-Pack grids of 5 × 5 × 1 and 5 × 3 × 1 were applied to sample the first Brillouin zone of the two slabs. All the ground-state atomic geometries were optimized by minimizing the Hellman-Feynman forces with the conjugate-gradient algorithm[42] until the total forces acting on each atom were converged better than 0.03 eV/Å. Transition-state geometries were located by using the minimum-mode following dimer method,[43] and the transition states were verified by frequency calculations in which only one imaginary frequency was obtained for each transition state.

In this work, adsorption energies (E_{ads}) were calculated relative to the energies of C and H in gas-phase methane and hydrogen, respectively, by using the formation energy approach[44-45]:

$$E_{\mathrm{ads}} = E_{\mathrm{surf+ads}} - E_{\mathrm{surf}} - \left(\alpha E_{\mathrm{C}} + \beta E_{\mathrm{H}}\right) \quad (1)$$

where $E_{\mathrm{surf+ads}}$ is the total energy of the surface with adsorbate adsorbed, E_{surf} is the total energy of the bare surface, E_{C} is calculated as $E_{\mathrm{methane(g)}} - 2E_{\mathrm{hydrogen(g)}}$, E_{H} is calculated as $0.5E_{\mathrm{hydrogen(g)}}$, and α and β represent the numbers of carbon and hydrogen atoms in the adsorbed species, respectively. It should be noted that, if all the energies in a given microkinetic model are referenced to the same set of reference energies, the variation in the reference states does not change the values of the reaction and activation energies, because the reference energies may cancel out in any relative quantities. In other words, the choice of the reference states is arbitrary, provided that the atomic references are associated with the same set of substances. This approach has the advantage of not distinguishing between adsorbate states and transition states, and because it ensures thermodynamic consistency, the use of the derived energies as inputs to a microkinetic model is preferred over other relative quantities.

2.2. Microkinetic Analysis

Microkinetic analysis in this work was carried out using a modified CatMAP code.[46] In general, the enthalpy (H°) and entropy (S°) were estimated under the ideal gas[47] (for gas-phase species) and harmonic (for reaction intermediates and transition states) approximations, as implemented in the ASE package.[48] The rate constant (k) of elementary steps was evaluated based on the transition state theory:[49]

$$k = \frac{k_{\mathrm{B}}T}{h} e^{-\Delta G^{\circ\ddagger}/k_{\mathrm{B}}T} \quad (2)$$

where h is Planck's constant, and $\Delta G^{\circ\ddagger}$ is the Gibbs free energy change from the initial state to the transition state. In the modified code, the entropy and enthalpy of the activated complex in molecular adsorption or desorption were assumed to be equal to the entropy of the adsorbed intermediate and the enthalpy of gas-phase species, respectively, which has previously been reported to be a reasonable approximation[49]. As a consequence, the Gibbs free energy of the activated complex for molecular adsorption and desorption can be written as

$$G_{\mathrm{TS}}{}^{\circ\ddagger} = H^{\circ}_{\mathrm{gas}} - T \cdot S^{\circ}_{\mathrm{ads}} \quad (3)$$

where $G_{\mathrm{TS}}{}^{\circ\ddagger}$ is the Gibbs free energy of the transition state, H°_{gas} is the enthalpy of gas-phase species, and S°_{ads} is the entropy of adsorbed species.

TOFs of elementary steps were determined by invoking the steady-state approximation and by numerically solving the coupled differential equations. The selectivity toward a specific product is defined as the rate of formation of the product in question divided by the rate of consumption of propane and weighted for the number of carbon atoms involved.

2.3. Experimental Methods

The alumina-supported monometallic Pt catalyst (Pt/Al_2O_3) used in this work was the same batch as in our previous study, which was prepared by the colloid method. The details of how the catalyst is prepared can be found in the literature.[50] The PDH assessments were performed in a μBenchCAT reactor (Altamira Instruments, USA) equipped with a quartz reactor (6 mm in diameter), and the products were analyzed online with a 4-channel micro-GC (INFICON 3000, USA). Typically, 0.05 g of catalyst was loaded in the quartz reactor. The experiments were conducted at $WHSV_{\mathrm{propane}}$ = 14.2 h^{-1} and a H_2/C_3H_8 molar ratio of 0, 1.25, 2.40, 3.56, 4.76, and 6.00, balanced with argon to achieve a total flow of 200 ml/min. The experiments were carried out at 723.15 K and atmospheric pressure with the same total flow and catalyst loading as above. Under these conditions, the influences of internal and external diffusion were safely

excluded. All the experiments were performed in a kinetic regime and with relatively low propane conversions (below 10.0%). The TOFs for propane consumption and propylene production were calculated by normalizing the mass activity to the number of surface Pt atoms which was determined by the H_2 chemisorption results. More details about the TOF calculation can be found in Section S1 in the Supporting Information. The selectivity toward gas-phase products was calculated based on the carbon mass balance.

3. RESULTS AND DISCUSSION

3.1. Energetics of PDH

The reaction network involving both the main and the side reactions of PDH is shown in Scheme 1, which is established based on the available experimental and theoretical findings.[9, 17, 20-21, 51-52] The 60 elementary steps can be divided into four groups: adsorption and desorption of gas-phase reactants and products, cleavage of C-H bond to form dehydrogenated species, deep dehydrogenation of adsorbed propylene or subsequent reaction intermediates, and C-C bond cracking of C3 and C2 species. The calculated Gibbs free energy barrier for each elementary step is given in Figure 1 and Table S1 in the Supporting Information, and the geometries of the transition states for propane (TS1 and TS2), 1-propyl (TS3 and TS4), and 2-propyl (TS5 and TS6) dehydrogenation are also shown in Figure 1. For the other elementary steps, the detailed information about the geometry of the transition state is presented in Figures S1 and S2 in the Supporting Information.

Scheme 1. Reaction Network for PDH[a]

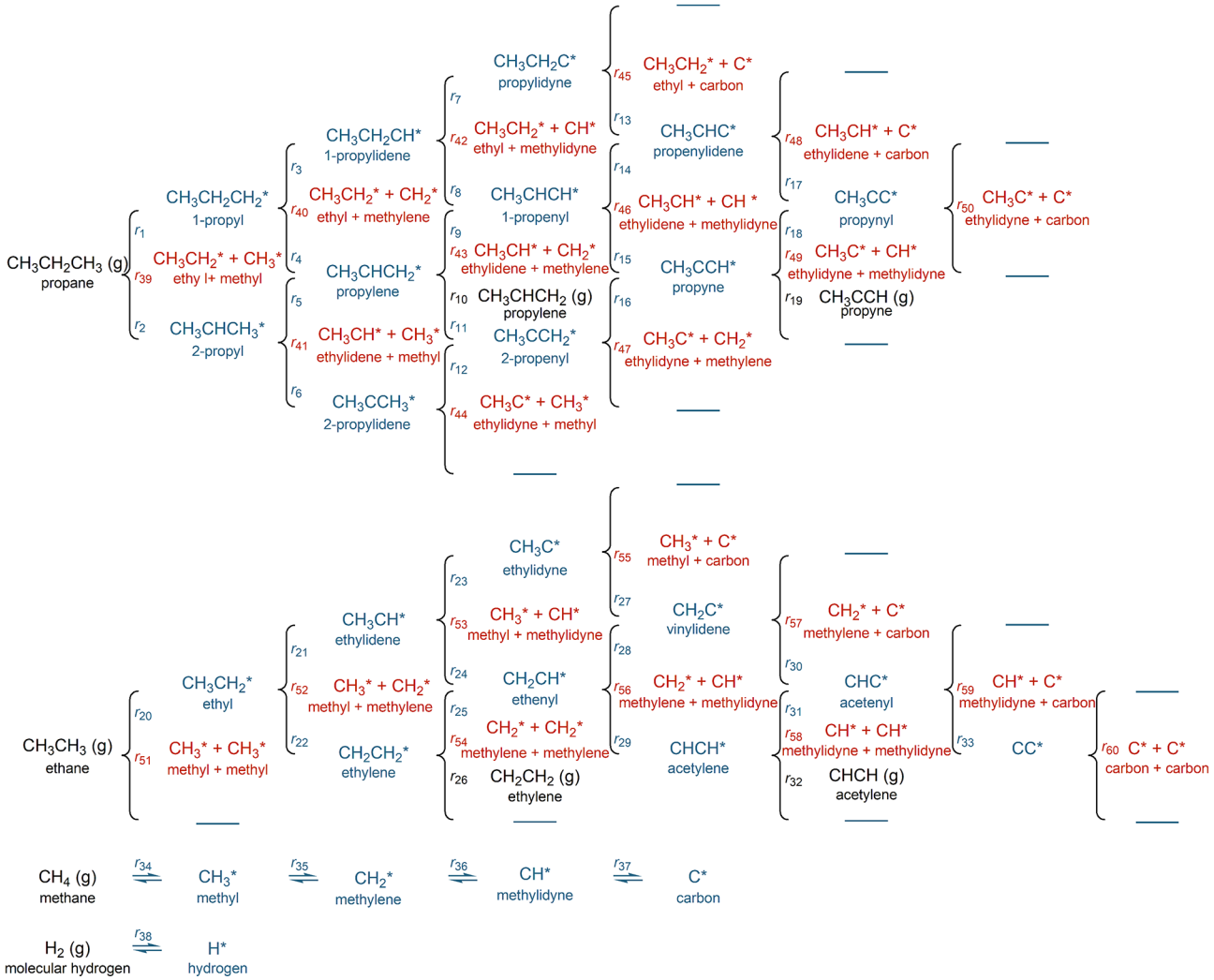

[a]All elementary steps are considered reversible.

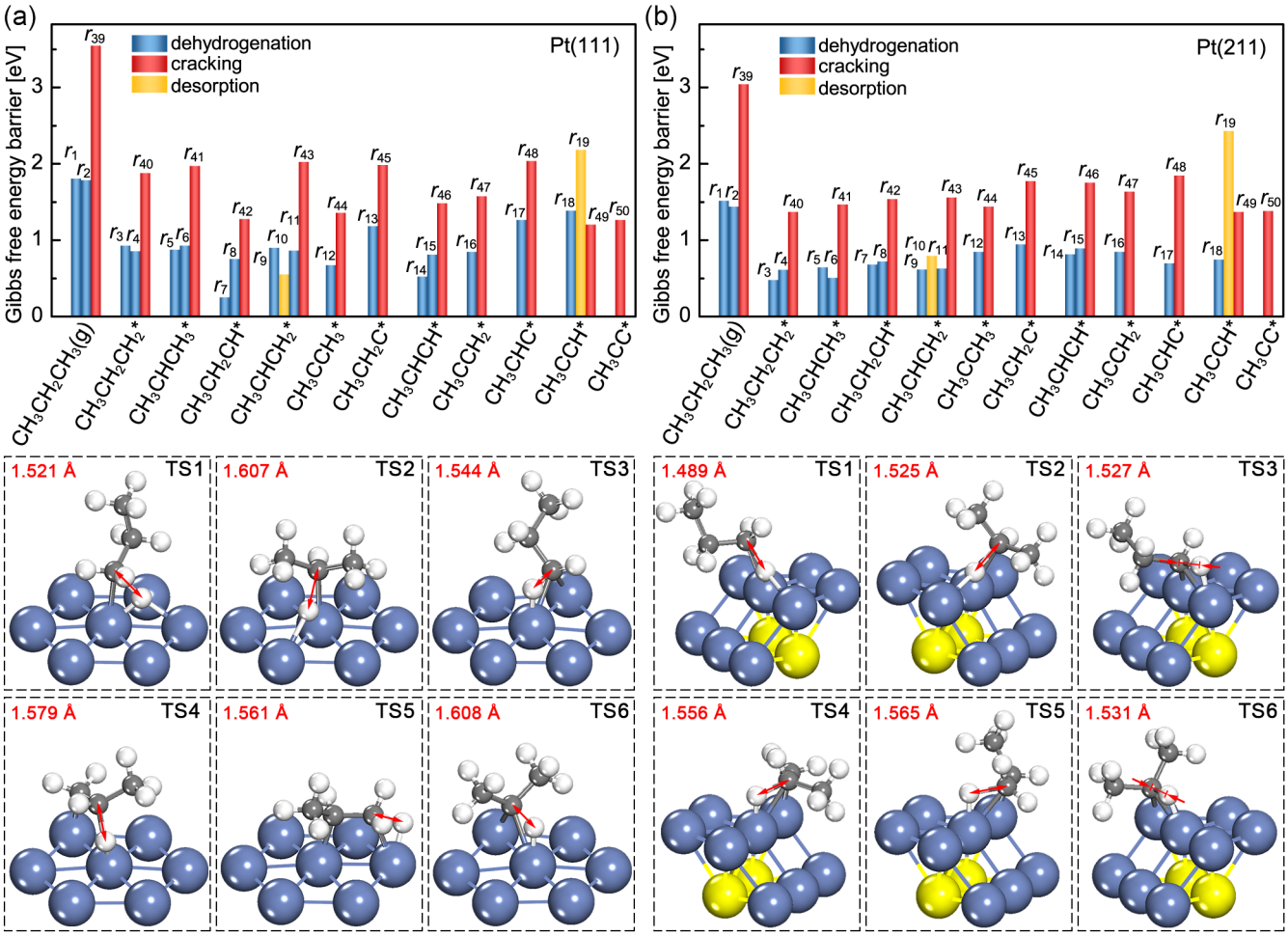

Figure 1. Gibbs free energy barriers (at 723.15 K) for dehydrogenation and cracking of C3 species in PDH over Pt(111) and Pt(211) and optimized geometries of transition states for propane (TS1 and TS2), 1-propyl (TS3 and TS4), and 2-propyl (TS5 and TS6) dehydrogenation. Elementary steps are defined in Scheme 1 and Table S1. The Pt atoms located below the outermost layer are colored yellow.

From the TS1 and TS2 in Figure 1a, it can be seen that on Pt(111) propane is dehydrogenated on top of a Pt atom, and the H atom detached from the C3 intermediates is relaxed to the Atop or Bridge site. The geometries of the transition states resemble the adsorption configurations of 1- and 2-propyl which are located at the most stable atop site (see Figure S3 in the Supporting Information). The Gibbs free energy barrier difference between the formation of 1-propyl via r_1 and 2-propyl via r_2 is only approximately 0.02 eV, indicating that the dehydrogenation of propane to $CH_3CH_2CH_2$* and CH_3CHCH_3* is equally favorable. Similarly, the transition states for the dehydrogenation of 1- and 2-propyl (TS3-TS6 in Figure 1a) are quite final-state like, and all the four reactions take place at the Bridge site. Furthermore, both 1- and 2-propyl tend to be dehydrogenated to propylene (via r_4 and r_5) instead of to 1- and 2-propylidene via r_3 and r_6, respectively, because the formation of propylene has lower forward Gibbs free energy barriers. From the analysis above, one can naturally conclude that the most kinetically preferred routes for propylene formation on Pt(111) are $r_1 \rightarrow r_4$ and $r_2 \rightarrow r_5$, which follows the generally accepted reverse Horiuti-Polanyi mechanism. Moreover, the adsorbed propyne is suggested to be the starting point for C-C bond breaking on Pt(111), which is due to the fact that CH_3CCH* is the sole C3 species that has a lower cracking barrier than the dehydrogenation barrier (1.20 *vs.* 1.38 eV for r_{49} and r_{18}, respectively, as shown in Figure 1a). These results obtained on Pt(111) are consistent with the previous theoretical studies using different DFT functionals such as PBE, opt-PBE vdW-DF, BEEF-vdW, *etc.*[9, 17, 20-21]

On Pt(211) all the six geometries of the TS1-TS6 resemble those over Pt(111), as shown in Figure 1b. However, the dehydrogenation reaction occurs by a completely different mechanism. As can be seen in Figure 1a-1b, the Gibbs free energy barriers for the dehydrogenation steps on the stepped surface are quite lower than those on the terrace surface, suggesting higher catalytic activity. In addition, the great difference between the Gibbs free energy barriers for propane activation to $CH_3CH_2CH_2$* via r_1 and to CH_3CHCH_3* via r_2 implies that the removal of the β-H from propane is kinetically preferred. Moreover, the high Gibbs free energy barriers for $CH_3CH_2CH_2$* and CH_3CHCH_3*

dehydrogenation to propylene compared to those for the formation of $CH_3CH_2CH^*$ and $CH_3CCH_3^*$ predict that both $CH_3CH_2CH_2^*$ and $CH_3CHCH_3^*$ are more likely to be converted to the deeply dehydrogenated species than to the target product propylene. To ensure that the use of the newly developed BEEF-vdW functional does not account for the observed deviation from the reverse Horiuti-Polanyi mechanism, another five widely used exchange-correlation functionals, including PBE, revPBE, optPBE-vdW, optB86b-vdW, and HSE06, were applied to verify the unexpected results. Since the relative magnitudes of the activation energies for the four aforementioned dehydrogenation steps play a key role in determining the pathway for propylene production, the dehydrogenation of $CH_3CHCH_3^*$ (r_5 and r_6) was taken as an example and the calculated energy barriers are presented and compared in Figure 2a. From the figure, one can see that the activation energy for β-H abstraction from $CH_3CHCH_3^*$ via r_6 is invariably lower than that for α-H abstraction via r_5, independent of the functionals used, which confirms that only a small amount of propane would be converted into propylene via r_4 and r_5 on Pt(211). Thus, it appears that there is an alternative to the commonly accepted mechanism for PDH on the corrugated Pt surface, which makes it difficult to identify the dominant reaction pathway from purely energetic considerations.

In addition, the Gibbs free energy barrier for CH_3CCH^* cracking is no longer lower than that for dehydrogenation (1.37 eV and 0.74 eV for r_{49} and r_{18}, respectively), which is in contrast to our previous PBE predictions.[17] Closer examination of the results indicates this difference arises from the different geometries of the transition state located for CH_3CCH^* dehydrogenation (r_{18}). As shown in Figure 2b, the activated complex may be found either at the fourfold hollow site of the step or at the step edge. The former structure resembles the adsorption configuration of CH_3CC^* (see Figure S4) and the latter is similar to that reported using the PBE functional[17]. The present work shows that both the BEEF-vdW and the PBE functionals give rise to virtually the same geometries of the two transition states and, regardless of the functional used, the dehydrogenation of CH_3CCH^* is likely to take place at the fourfold hollow site of the step rather than occurring at the step edge, because the transition-state energy for the latter process is 0.90 and 0.79 eV less negative for the BEEF-vdW and PBE functional, respectively. Given the fact that the dehydrogenation reaction is kinetically more favorable than the cracking reaction for all the C3 species except CH_3CC^* (see Figure 1b), CH_3CC^* is predicted to be the starting point for C-C bond breaking on Pt(211).

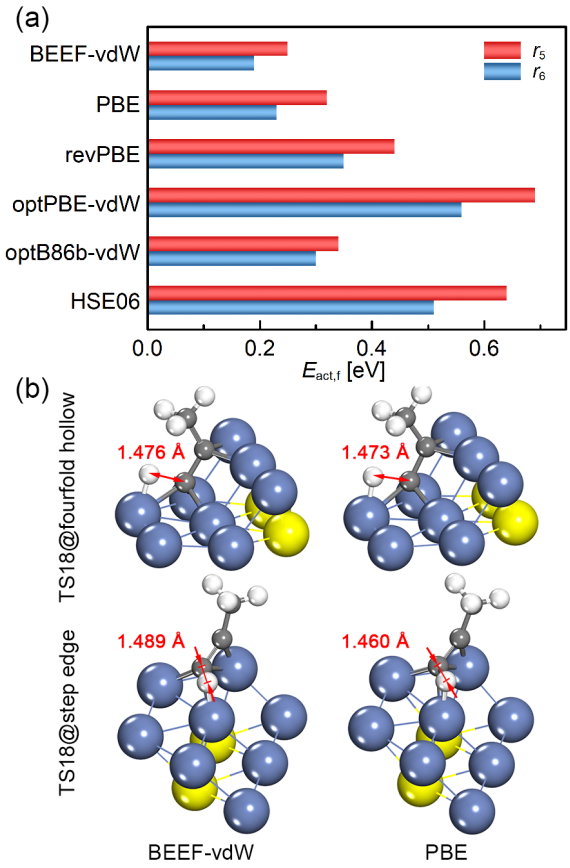

Figure 2. (a) Activation energies ($E_{act,f}$) for 2-propyl dehydrogenation to propylene via r_5 and to 2-propylidene via r_6 over Pt(211) as calculated by using different exchange-correlation functionals; (b) two different transition states for CH_3CCH^* dehydrogenation (TS18) over Pt(211) as obtained by both the BEEF-vdW and the PBE functionals.

3.2. Experimentally Determined Kinetics of PDH

Because PDH has a very complex mechanism, the analysis of energetics alone cannot give much physical insight and a comprehensive microkinetic analysis is highly desired. To gain confidence in the results of the microkinetic analysis, at least several key aspects of the theoretical predictions need to be validated and confirmed by experimental data. In this work, the experimentally determined PDH kinetics was obtained on Pt nanoparticles of around 5.0 nm in size, and the details of catalyst characterization can be found in our previous work[50] and in Figure S5 in the Supporting Information.

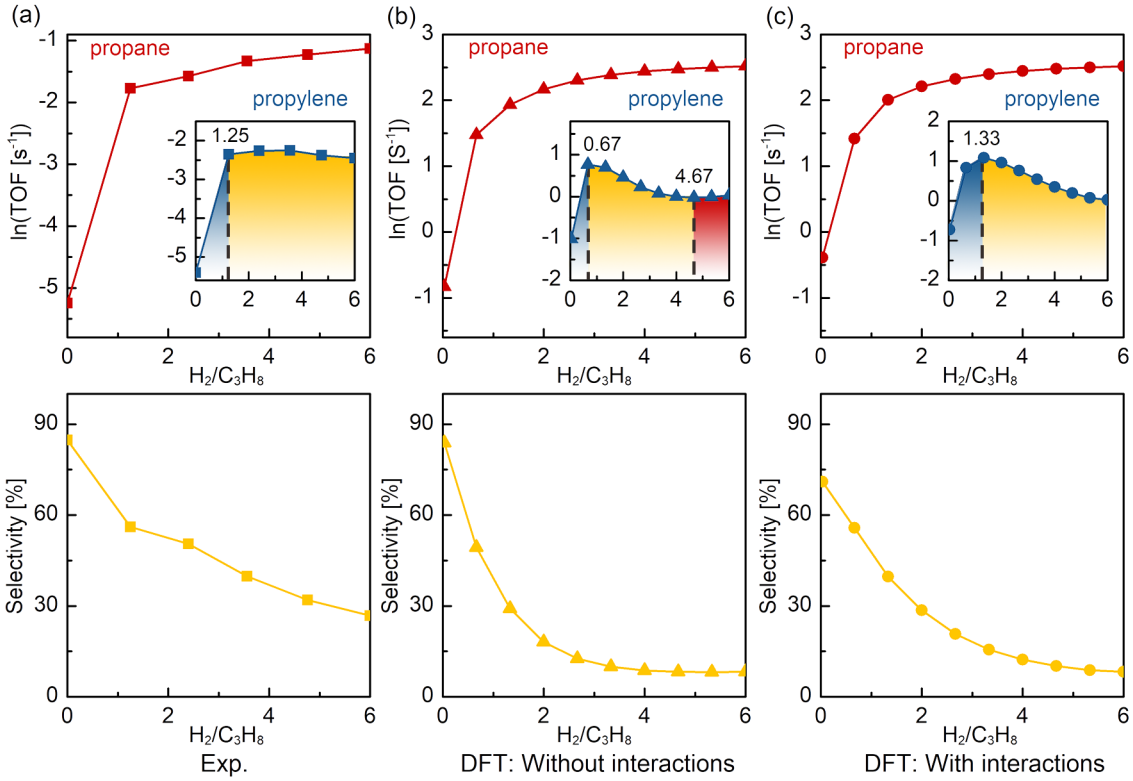

Figure 3. Plots of TOFs for propane consumption and propylene production and of propylene selectivities over 5 nm Pt nanoparticles obtained (a) in experiment and from microkinetic analysis (b) without and (c) with adsorbate-adsorbate interactions as a function of the H_2/C_3H_8 ratio at 723.15 K and 0.03 bar of propane.

The H_2/alkane ratio is generally used to investigate the effect of H_2 co-feeding with alkane on the catalytic activity and alkene selectivity, where the H_2 and inert flow rates are varied while the alkane and total inlet flow rates are held constant.[21, 53-55] The experimental results in Figure 3a indicate the TOF for propane consumption (TOF_{propane}) is increased by 10 times when hydrogen is introduced into the inlet stream with the H_2/C_3H_8 ratio of 1.25 and continues to increase with increasing the ratio. The positive effect of co-feeding of hydrogen with propane on the activity of PDH has previously been reported in the literature,[22, 54] which suggested that the co-feeding can suppress coke formation through the hydrogenation of coke precursor species and therefore maintain the catalytic activity over Pt catalyst.

As for the production of propylene, the dependence of the TOF ($TOF_{\text{propylene}}$) on the H_2/C_3H_8 ratio exhibits a distinctly different pattern, where the rate first shows positive hydrogen pressure dependence and then the rate law has a negative reaction order in hydrogen when more hydrogen continues to be added into the inlet stream. It is important to note that we have ensured the amount of propylene in the gas mixture is much less than its equilibrium concentration throughout the reaction (see Figure S6 in the Supporting Information) and the experiments have been carried out in the kinetic regime. The observation that the curve goes through an inflection point at the H_2/C_3H_8 ratio of around 1.30 has previously been reported,[21, 54] not only in PDH but also in the dehydrogenation of ethane and butane on various Pt-based catalysts;[54-56] that is, it is a characteristic feature of the kinetics of the dehydrogenation of light alkanes over Pt.

Furthermore, it is found that the co-feeding of hydrogen has a negative effect on the selectivity towards propylene ($S_{\text{propylene}}$). Specifically, as the H_2/C_3H_8 ratio increases from 0 to 6, the $S_{\text{propylene}}$ decreases monotonically from 84.8% to 26.8%, implying an increase in the selectivity towards C2 and C1 species (see Figure S7 in the Supporting Information). The explanation is probably that the hydrogenolysis reaction has a more positive reaction order in hydrogen than the dehydrogenation reaction, and the increase in the hydrogen content would promote the side reaction more dramatically. Through microkinetic analysis, however, Saerens et al.[21] predicted that the propylene selectivity on the Pt(111) surface should not be much influenced by the increased H_2/C_3H_8 inlet ratio, and Lian et al.[20] claimed by carrying out kinetic Monte Carlo simulations that the selectivity toward propylene can even be increased with the introduction of H_2 over Pt(111). Therefore, the computational work so far seems to have difficulty in properly reproducing the experimentally determined kinetics of PDH.

3.3. Microkinetic Analysis without Adsorbate-Adsorbate Interactions

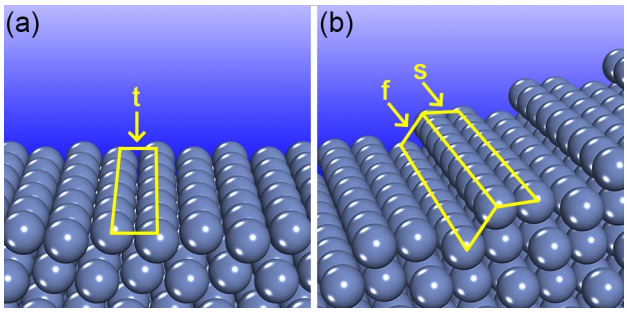

Figure 4. Schematic representations of active sites on (a) Pt(111) and (b) Pt(211). On Pt(111), adsorbates occupying the sites labeled with "t" refer to adsorption at the terrace sites. On Pt(211), adsorbates occupying the sites labeled with "s" and "f" refer to adsorption at the step and fourfold hollow sites, respectively.

Based on Scheme 1, a microkinetic model is constructed and solved by invoking the steady-state approximation (see Section S5 in the Supporting Information for details). In the kinetic model, Pt(111) is viewed as composed of terrace (labelled with "t") sites and Pt(211) is thought of as comprising two types of active sites, namely, fourfold hollow (labelled with "f") and step (labelled with "s") sites, as shown in Figure 4. The reasoning behind the site definition is that, in more detailed DFT calculations, CH_3CC*, CHC*, and CC* are found to prefer the fourfold hollow site of the step while the other species are bound more strongly at the step edge (see Figure S4 in the Supporting Information). In addition, a hydrogen reservoir site is considered on both Pt(111) (labeled with "ht") and Pt(211) (labelled with "hs"), which is based on the assumption that atomic hydrogen is so small that its adsorption is independent of the adsorption of other species (that is, the interactions between hydrogen and other species are negligibly small, giving rise to non-competitive adsorption).[57-58]

In this work, the catalytic behavior of supported Pt catalysts was interpreted in terms of a multi-faceted kinetic model, where the coordinatively saturated (terraces) and unsaturated (steps/edges) active sites are represented by the close-packed (111) and stepped (211) surfaces, respectively. For simplicity, a "no diffusion" model[59] was used, in which the reaction is considered to take place independently on Pt(111) and Pt(211). Thus, the calculated TOFs on Pt nanoparticles can be obtained by using a linear combination of the TOF on each surface. Because nanoparticles of different sizes and shapes have different relative occurrence of active sites of various types, the TOFs were evaluated on the assumption that the 5.0 nm Pt nanoparticles have an icosahedral shape (see Figure S8 in the Supporting Information).[60-61] It is worth noting that no effort has been devoted to fitting the simulation data to the experiments.

Here we first conducted microkinetic analysis without adsorbate-adsorbate interactions to reveal the kinetics of PDH over Pt, and the results are presented in Figure 3b. It is found that the inflection point of the plot of $TOF_{\text{propylene}}$ occurs at a H_2/C_3H_8 ratio of 0.67, which is much lower than that found in experiment. More importantly, there is an unexpected increase in the $TOF_{\text{propylene}}$ and $S_{\text{propylene}}$ at high H_2/C_3H_8 ratios, which is absent in the experimental results. As mentioned in the Introduction, the neglect of lateral adsorbate-adsorbate interactions is the most likely reason for the discrepancies between the simulated and experimental kinetics. As illustrated in Figure 5a, the active sites are considerably blocked by the abundant reaction intermediates, such as CH_t and C_t at the "t" site, CH_s and C_s at the "s" site, and CHC_f at the "f" site (the values of the coverages determined from the microkinetic model without adsorbate-adsorbate interactions are included in Section S7 in the Supporting Information), indicating that there must exist strong adsorbate-adsorbate interactions. These interactions have great influences on the surface coverages and chemisorption strengths of reaction intermediates and are the major factors affecting the accuracy of the predicted kinetics.

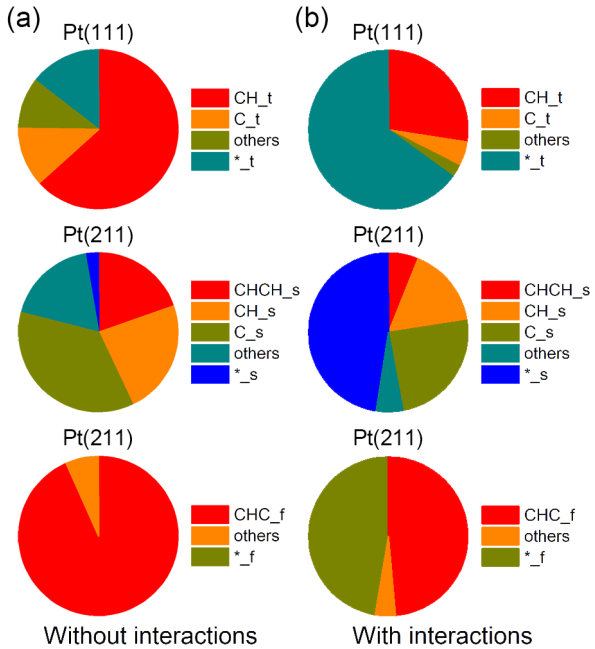

Figure 5. Surface coverages of species at the "t", "s", and "f" sites obtained from the microkinetic model (a) without and (b) with adsorbate-adsorbate interactions at 723.15 K, 0.03 bar of propane, and H_2/C_3H_8 = 0.03.

3.4. Microkinetic Analysis Including Adsorbate-Adsorbate Interactions

In light of this fact, adsorbate-adsorbate interactions were then included in our microkinetic model. Previously, Saerens et al.[21] constructed a coverage-dependent simulation by co-adsorbing hydrogen with other species to study the effect of the hydrogen coverage on the catalyst performance in PDH. They found that the reaction activity is about 3 times lower than in the model without hydrogen co-adsorption, and the H_2/C_3H_8 feed ratio at which the highest rate for the propylene production is attained changes from 3.0 to 1.5. Lian et al.[20] also evaluated the lateral interactions between adsorbates by cluster expansion Hamiltonians, and the lateral interactions of up to 0.4 eV were observed between C1 intermediates. In our model, the self-interactions of 11 reaction intermediates including C_t, CH_t, and CH_3C_t on Pt(111) and C_s, CH_s, CHCH_s, CH_2C_s, CH_3C_s, CC_f, CHC_f, and CH_3CC_f on Pt(211) are considered, for their coverages are predicted to be greater than 0.01 ML at the H_2/C_3H_8 ratio of 0.03 by microkinetic analysis without adsorbate-adsorbate interactions. In addition, the cross-interactions between CHC_f and 29 species are also included, consisting of (i) the abundant reaction intermediates including C_s, CH_s, CH_2C_s, CH_3C_s, CC_f, and CH_3CC_f, (ii) the transition states for the dehydrogenation of C3 species, the cracking of CH_3CCH_s and CH_3CC_f, and (iii) the adsorbed CH_3CHCH_2_s, CH_3CCH_s, CH_2CH_2_s, and CHCH_s. Other interactions between the species involved are negligibly small and neglected, which is a commonly used strategy for describing the kinetics of complex reactions involving a large number of elementary steps and reaction intermediates.[62-63]

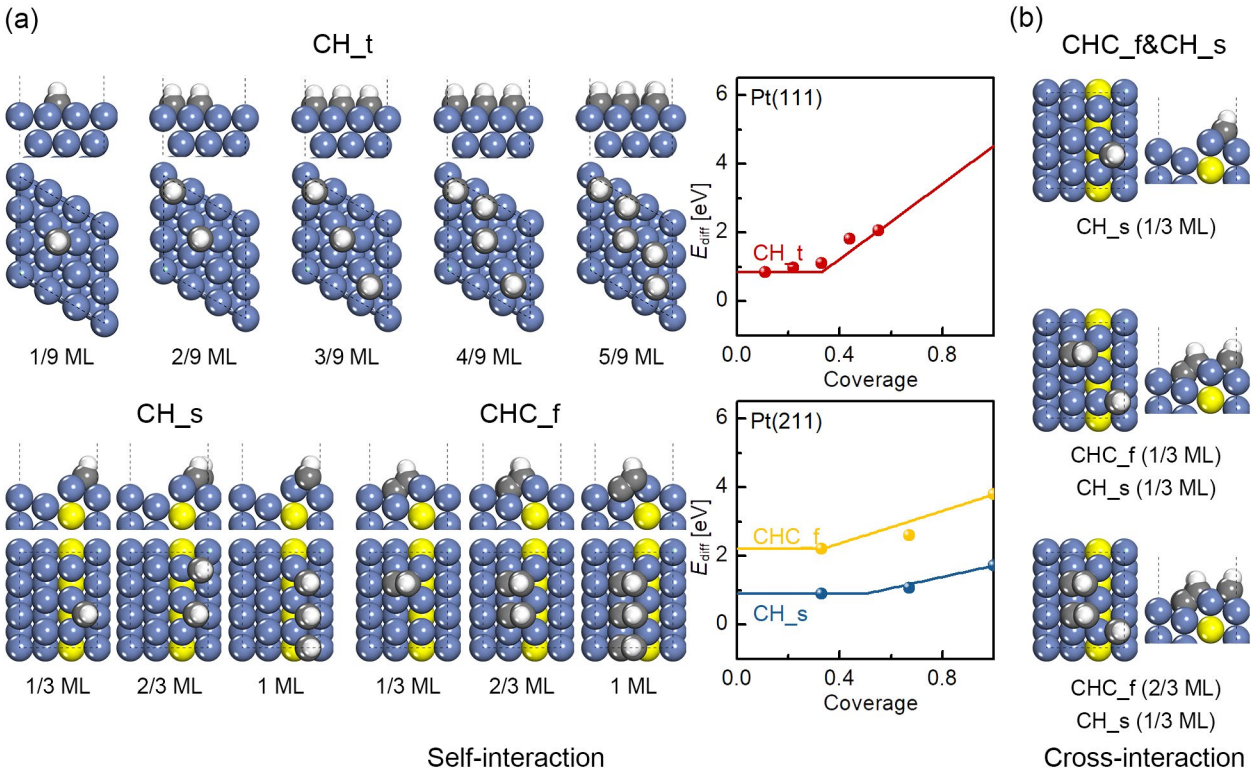

Figure 6. (a) Adsorption configurations of CH_t, CH_s, and CHC_f at different coverages and the corresponding coverage-dependent differential adsorption energies. The points represent the energies computed using DFT and the solid lines represent the energies obtained from the second-order adsorbate-adsorbate interaction model; (b) adsorption configurations of CH_s at the CHC_f coverages of 0, 0.33, and 0.67 ML.

The lateral adsorbate-adsorbate interactions were modeled using a second-order expansion of the integral adsorption energy in terms of the coverage:

$$E_{\text{int}} = \sum_i E^0_{\text{diff},i}\theta_i + \frac{1}{2}\sum_s \sum_q f^2_{sq} \sum_{i\in s}\sum_{j\in q} \varepsilon_{ij}\theta_i\theta_j \quad (4)$$

where E_{int} is the integral adsorption energy on a surface, which is a function of the coverages of all the reaction intermediates, $E^0_{\text{diff},i}$ is the differential adsorption energy of species i in the low-coverage limit, f_{sq} is a piecewise-linear function for the energy as a function of the coverages at the adsorption sites s and q, and ε_{ij} is a matrix of parameters for the interaction between species i and j, which was determined by fitting the interaction model to the DFT-calculated data (see below). The differential adsorption energy can be obtained by differentiating Eq. 4 with respect to surface coverage:

$$\begin{aligned} E_{\text{diff},k}(\theta_k) &= \frac{\partial E_{\text{int}}}{\partial \theta_k} \\ &= E^0_{\text{diff},k} + \sum_s f^2_{sq_k} \sum_{i\in s} \varepsilon_{ik}\theta_i + 2\sum_s f_{sq_k} f'_{sq_k} \sum_{i\in s}\sum_{j\in q_k} \varepsilon_{ij}\theta_i\theta_j \end{aligned} \quad (5)$$

where $E_{\text{diff},k}$ is the differential adsorption energy of species k, f'_{sq} is the derivative of f_{sq} with respect to the total coverage at sites s and q, and q_k denotes the site q with species k adsorbed.

The value of ε_{ij} was obtained by minimizing the error function using the downhill simplex algorithm:

$$f = \frac{\sum_{i=1}^{N}\left(\left|E^{\text{DFT}}_{\text{int}} - E_{\text{int}}\right| + \left|E^{\text{DFT}}_{\text{diff}} - E_{\text{diff}}\right|\right)_i}{N} \quad (6)$$

where N is the number of DFT data used to fit each interaction parameter, $E^{\text{DFT}}_{\text{int}}$ and $E^{\text{DFT}}_{\text{diff}}$ are the integral and differential adsorption energies estimated by DFT calculations, respectively:

$$E^{\text{DFT}}_{\text{diff}}(\theta) = E_{\text{ads}}(\theta) - E_{\text{ads}}(\theta - \Delta\theta) \quad (7)$$

$$E^{\text{DFT}}_{\text{int}}(\theta) = E^{\text{DFT}}_{\text{diff}}(\theta)\cdot \Delta\theta + E^{\text{DFT}}_{\text{int}}(\theta - \Delta\theta) \quad (8)$$

where $\Delta\theta$ is the change in surface coverage after introducing an adsorbate. When $\theta = \Delta\theta$, $E^{\text{DFT}}_{\text{diff}}(\Delta\theta) = E_{\text{ads}}(\Delta\theta)$ and $E^{\text{DFT}}_{\text{int}}(\Delta\theta) = E^{\text{DFT}}_{\text{diff}}(\Delta\theta)\cdot\Delta\theta$. Substitution of ε_{ij} into Eq. 5 yields the differential adsorption energy of each intermediate as a function of the surface coverage, which is then used as an input to the microkinetic model. More technical details of the interaction model are included in Section S8 in the Supporting Information and the literature.[64]

Several representative adsorption and co-adsorption configurations as a function of the site coverage are shown in Figure 6a and 6b, respectively. As indicated in Figure 6a, the interaction model predicts with reasonable accuracy the DFT-calculated coverage-dependent differential adsorption energy. Comparison between Figure 5a and 5b reveals that, with the consideration of the repulsive adsorbate-adsorbate interactions, the coverages of the abundant reaction intermediates are substantially decreased and many active sites originally blocked are now ready for adsorption (the values of the coverages determined from the microkinetic model with adsorbate-adsorbate interactions are included in Section S9 in the Supporting Information). Importantly, the experimentally determined kinetics of PDH over 5 nm Pt nanoparticles can be well reproduced by the microkinetic analysis with adsorbate-adsorbate interactions, as can be seen in Figure 3c. In particular, the inflection point of the plot of $TOF_{\text{propylene}}$ is predicted to be at the H_2/C_3H_8 ratio of 1.33, which is very close to the experimental observation. Furthermore, although the predicted TOFs are higher than the experimental values, the dependences of the catalytic activity and catalyst selectivity on the H_2/C_3H_8 ratio (especially at the high values) apparently follow the same trend as that exhibited in experiment. The overestimated TOFs have also been reported by Saerens et al.[21] and Lian et al.[20] One of the possible reasons can be traced to the overestimation of the rate constants by the transition state theory, which is associated with the "recrossings" that cross back into the reactant region on the potential energy surface and are miscounted as reactive events.[65] Another reason is that the simulations are conducted on clean Pt surfaces, while in reality the strongly adsorbed species could partially occupy the active sites, thus impairing the catalytic activity.

The detailed results from the microkinetic analysis over Pt(111) and Pt(211) are shown in Figure 7a. It is found that the activity of Pt(211) is orders of magnitude greater than that of Pt(111), which can be explained by the lower apparent activation energy on Pt(211). From Figure 7b, one can see that the calculated apparent activation energy on Pt(211) is 0.20 eV at a H_2/C_3H_8 ratio of 1.00, which is 0.49 eV lower than that on Pt(111). These findings are in accord with the experimental observations by Zhu et al,[12] who proposed that the activation energy for PDH increases with increasing Pt cluster size and therefore with increasing the fraction of terrace sites. As a result, the catalytic behavior of the 5 nm sized Pt catalyst is suggested to be dominated by Pt(211), although Pt(111) has a much higher mole fraction on the catalyst surface (approximately 74.0 %, see Section S6 in the Supporting Information).

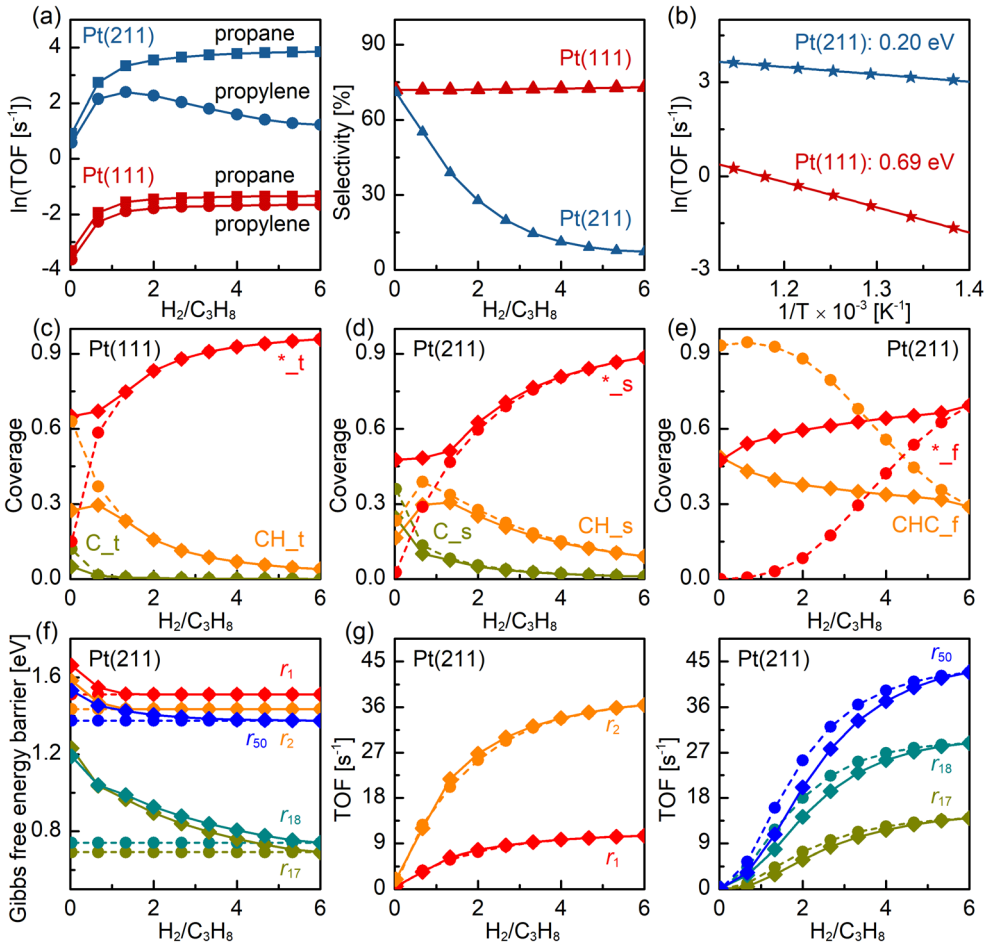

Figure 7. (a) Plots of TOFs for propane consumption and propylene production and of propylene selectivities over Pt(111) and Pt(211) obtained from the microkinetic analysis with adsorbate-adsorbate interactions as a function of the H_2/C_3H_8 ratio at 723.15 K and 0.03 bar of propane; (b) apparent activation energy for propane consumption over Pt(111) and Pt(211); (c-e) coverages of free sites and abundant reaction intermediates on Pt(111) and Pt(211) and (f-g) Gibbs free energy barriers and TOFs for propane activation (r_1 and r_2) and CH_3CC_f formation and cracking (r_{17}, r_{18}, and r_{50}) reactions on Pt(211) obtained from microkinetic analysis without (dashed line) and with (solid line) adsorbate-adsorbate interactions.

In addition, the rate for propane consumption increases as the H_2/C_3H_8 ratio goes up on both the Pt(111) and the Pt(211) surfaces (see Figure 7a). It is found that the increase in the TOF_{propane} does not bear any direct relation to the variation in the dehydrogenation barrier caused by the interaction between H and other adsorbed species or activated complexes, because the coverage of hydrogen is invariably low under all the reaction conditions concerned (see Figure S10 in the Supporting Information). Rather, at low inlet H_2/C_3H_8 ratios, it is closely related to the increased coverage of free sites (see Figure 7c-7e) and to the lowered coverage-dependent energy barriers for propane activation (see Figure 7f). Without H_2 co-feeding, high coverages of the deeply dehydrogenated coke precursors, particularly CH_t and C_t on Pt(111) and CH_s, C_s, and CHC_f on Pt(211), and high Gibbs free energy barriers for propane dehydrogenation (r_1 and r_2) are observed, which give rise to the low activity. As the partial pressure of H_2 rises, the abundant reaction intermediates would be readily removed as by-products through hydrogenation, making more active sites ready to activate C-H bonds. As can be seen in Figure S11 in the Supporting Information, the increased H_2/C_3H_8 ratio has a positive effect on the rates for CH and C hydrogenation to CH_2 and CH and on the rate for CHC_f cracking to CH_s and C_s, thus promoting the formation of methane. More importantly, the increase in the coverage of free sites in turn leads to the lowered Gibbs free energy barriers for C-H bond breaking. For instance, when the H_2/C_3H_8 ratio increases from 0.03 to 0.67, the Gibbs free energy barriers for r_1 and r_2 decrease from 1.66 and 1.58 eV to 1.55 and 1.47 eV on Pt(211), respectively. Thus, in principle, the essential role of the increased H_2/C_3H_8 ratio at low values is to give rise to more active sites by gasifying adsorbed C1 and C2 species, lower the dehydrogenation barriers, and hence achieve a long-term stability of the catalyst. It should be noted that, when the H_2/C_3H_8 ratio continues to increase, the coverage of free sites may exceed the

threshold values at which adsorbate-adsorbate interactions can be neglected, and for then the Gibbs free energy barriers begin to remain constant and the increased TOF_{propane} with increasing the H_2/C_3H_8 ratio is attributed solely to the increased coverages of free sites.

On the other hand, the effect of the H_2/C_3H_8 ratio on the rate for propylene production differs greatly on Pt(111) and Pt(211), as can be seen in Figure 7a. On Pt(111) the $TOF_{\text{propylene}}$ continues to increase with increasing the H_2/C_3H_8 ratio and the $S_{\text{propylene}}$ is found to be insensitive to the change in the partial pressure of H_2. By comparison, the $TOF_{\text{propylene}}$ on Pt(211) first increases to a maximum at the H_2/C_3H_8 ratio of 1.33 and then declines, in remarkably good agreement with experiment. Meanwhile, the propylene selectivity decreases steadily with the H_2/C_3H_8 ratio, bearing close resemblance to the experimentally determined kinetics. These important differences and similarities, together with the fact that Pt(211) shows a much stronger activity, suggest that under-coordinated Pt atoms cannot be completely deactivated under realistic reaction conditions and would even play a dominant role in catalyzing PDH.

It should be noted that the characteristic feature of the PDH kinetics on Pt can only be properly reproduced by the microkinetic analysis with the inclusion of the lateral adsorbate-adsorbate interactions on the stepped surface. The improvement in the reproduction of the experimentally determined kinetics (particularly the inflection point of the $TOF_{\text{propylene}}$ curve) benefits from the more accurately predicted surface coverages and energetics. In the microkinetic model without adsorbate-adsorbate interactions, the Gibbs free energy barriers do not change with the surface coverages of the adsorbates. As the H_2/C_3H_8 ratio rises, the increase in the coverage of *_s would speed up the consumption of propane (r_1 and r_2), while the growth in the coverage of *_f accelerates the rate of the deep dehydrogenation and cracking reactions (e.g., CH_3CC_f formation via r_{17} and r_{18}). The inflection point of the plot of $TOF_{\text{propylene}}$ occurs at the H_2/C_3H_8 ratio of 0.67 (see Figure S12 in the Supporting Information) where the negative effect of the increased *_f coverage begins to dominate the positive effect of the increased *_s coverage.

When the repulsive interactions are included in the kinetic model, the Gibbs free energy of activation, and hence the rate constant, becomes coverage-dependent (see Figure 7f). In particular, when the surface coverages of the "s" and "f" sites exceed the threshold values of 0.50 and 0.33 ML, respectively, the Gibbs free energy barriers for bond-breaking reactions are raised as a result of the weakened bonding of the adsorbates to the surface. Thus, the variation in the kinetics depends upon the changes both in the surface coverages and in the rate constants. As can be seen in Figure 7d-7e, the coverage of adsorbates is lowered due to the repulsive lateral interactions between them, but the increased Gibbs free energy barriers (see Figure 7f) almost counteract the effect of the increased coverage of *_s on the rate of the main reaction of PDH, as shown in Figure 7g. For the side reaction, however, the rate at a given H_2/C_3H_8 ratio is generally lower than that without including adsorbate-adsorbate interactions (see Figure 7g) because the effect of the decreased rate constant dominates the effect of the increased coverage of *_f. Interestingly, the difference in the side reaction rate becomes greater as the H_2/C_3H_8 ratio increases to 2 and then goes down. Given the fact that the main reaction rate does not change very much, the inhibition of the side reaction by the presence of adsorbate-adsorbate interactions, especially at low H_2/C_3H_8 ratios, leads to the optimum H_2/C_3H_8 ratio shifting to a higher value (1.33), causing it to be much closer to the experimental observation.

Furthermore, the unexpected increase in the $TOF_{\text{propylene}}$ at very high H_2/C_3H_8 ratios (> 4.67, see Figure S12) on Pt(211) can be eliminated by including the interactions between the species adsorbed at the "f" site. It is found that the reduction in the coverage of CHC_f plays a dominant role in lowering the Gibbs free energy barriers for the side reactions (eg., r_{17}, r_{18}, and r_{50}) with increasing the H_2/C_3H_8 ratio. At the high ratios, the coverage of *_s is above 0.50 ML and the adsorbate-adsorbate interactions have no effect on the main reaction; meanwhile, the side reaction rate increases faster than that in the absence of the lateral interactions, mainly because the weakening of the interaction of CHC_f with other species becomes more pronounced when there are more free "f" sites available for bonding, and hence the Gibbs free energy barriers are less increased. For this reason, only when the adsorbate-adsorbate interactions are taken into consideration can we predict with reasonable accuracy the dependence of the production rate of propylene on the H_2 partial pressure.

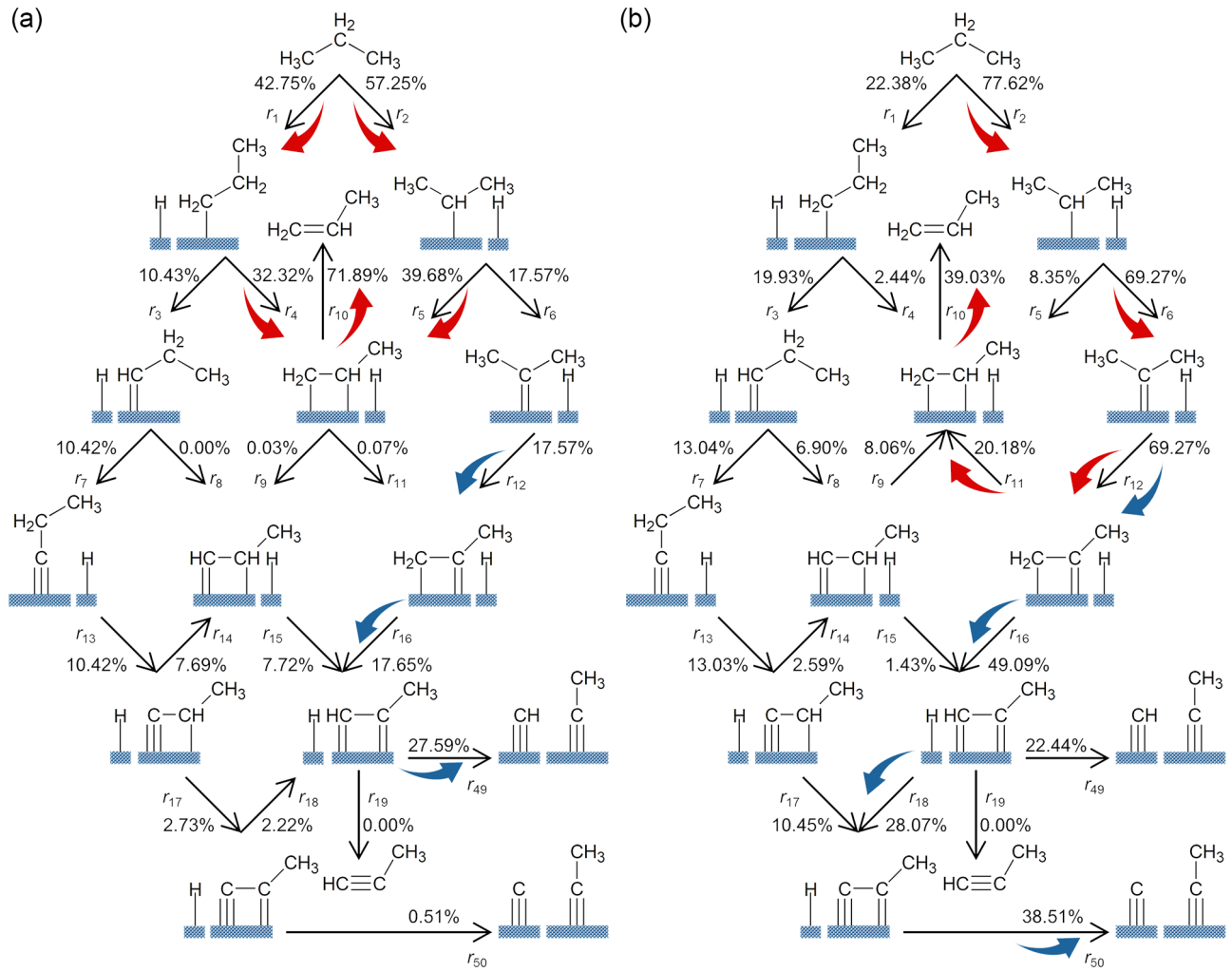

Figure 8. Flux analysis of PDH under experimental reactor inlet conditions (723.15 K, 0.03 bar of propane, and 0.04 bar of hydrogen) over (a) Pt(111) and (b) Pt(211) with adsorbate-adsorbate interactions considered. The arrows which are labelled with the percentage of the total reaction flux indicate the direction in which the reversible elementary steps actually proceed. The percentage of the reaction flux is calculated as the absolute value of the net rate for that elementary step divided by the rate for propane consumption.

3.5. Reaction Mechanism

3.5.1. Flux Analysis

Having obtained a reasonably reliable description of the PDH kinetics, we are now in a position to formulate the reaction mechanism. The flux analysis of the reaction has been performed at 723.15 K and the optimum H_2/C_3H_8 ratio of 1.33 over both Pt(111) and Pt(211), as illustrated in Figure 8. On Pt(111) the dominant pathways for propylene production (see the red arrows in Figure 8a) are found to be along $r_1 \rightarrow r_4$ and along $r_2 \rightarrow r_5$, which agrees completely with our energetic analysis in Section 3.1 and further demonstrates that the production of propylene on Pt(111) follows the well-known reverse Horiuti-Polanyi mechanism. In addition, the flux analysis confirms that the formation of by-products arises primarily from the cracking of CH_3CCH_t via r_{49}, as indicated by the blue arrows in Figure 8a. Moreover, it is found that CH_3CCH_t comes mainly from the deep dehydrogenation of $CH_3CH_2CH_2\_t$ and $CH_3CHCH_3\_t$ via r_3 and r_6, respectively, rather than from the dehydrogenation of propylene via r_9 and r_{11}. Therefore, the formation of propylene and by-products proceeds essentially by way of two parallel reactions starting from $CH_3CHCH_3\_t$. In light of this fact, the reaction network on Pt(111) is simplified in Scheme 2.

Scheme 2. Simplified Reaction Network for PDH over Pt(111) and Pt(211)

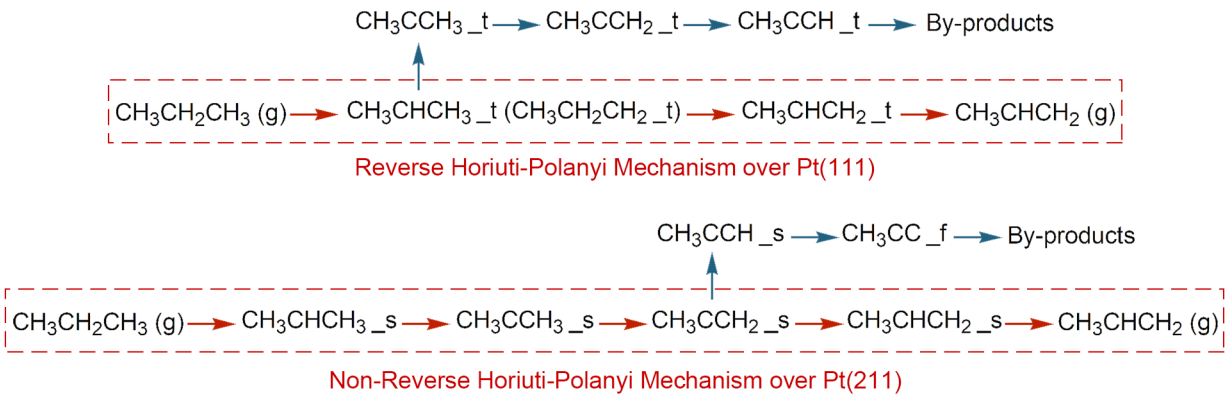

On Pt(211), it is interesting to find that, in addition to the two pathways mentioned above, a third route that proceeds by a non-reverse Horiuti-Polanyi mechanism (see the red arrows in Figure 8b) contributes to the PDH kinetics as well, which is composed of three dehydrogenation steps followed by one hydrogenation step ($r_2 \rightarrow r_6 \rightarrow r_{12} \rightarrow r_{11}$). More importantly, this pathway accounts for more than half (51.70%) the propylene production and therefore plays a dominant role on Pt(211). Detailed analysis indicates that the initial dehydrogenation of propane via r_2 is preferred over r_1 and 77.62% of propane is dehydrogenated to CH_3CHCH_3_s. However, only 10.76% of the CH_3CHCH_3_s species are converted into propylene via r_5 and most of them are dehydrogenated to CH_3CCH_3_s and then further to CH_3CCH_2_s. Finally, 29.13% of CH_3CCH_2_s are hydrogenated to form 51.07% propylene via r_{11}. It is important to note that this plausible reaction mechanism persists and dominates even at higher temperatures and pressures (see Figure S13 in the Supporting Information). On this stepped surface, the cleavage of C-C bonds is more likely to occur in CH_3CC_f via r_{50} (see the blue arrows in Figure 8b) than in CH_3CCH_s, in accord with the predictions from energetic analysis. At the H_2/C_3H_8 ratio of 1.33, although the Gibbs free energy barrier for CH_3CCH_s dehydrogenation is raised by 0.25 eV by the presence of the adsorbate-adsorbate interactions, its value remains lower than the almost unchanged cracking barrier of CH_3CCH_s, which is in contrast to the results on Pt(111) where the C-C bond breaking in CH_3CCH_t is kinetically preferred. In much the same way, the reaction network for PDH over Pt(211) is also simplified in Scheme 2. It can be seen that the side reaction competes with the main reaction at CH_3CCH_2 rather than at CH_3CHCH_3.

To see if the reaction mechanism would change significantly as the H_2/C_3H_8 ratio is varied, the flux analysis has been carried out under different reaction conditions. On Pt(111), increasing the H_2/C_3H_8 ratio would promote the forward reaction of r_4 and r_5, thus producing adsorbed propylene more rapidly, as can be seen in Figure 9a. Meanwhile, the reverse reaction of r_{49} is inhibited more dramatically than the forward reaction, leading to an increased CH_3CCH_t cracking rate and, consequently, to an increase in the by-product formation. As a result, the percentages of the reaction flux for both propylene production and C3 cracking do not change very much (see Figure 9a); that is, the dominant propylene production pathways observed at the H_2/C_3H_8 ratio of 1.33 invariably make major contributions to the production of propylene even if the H_2 partial pressure is changed.

On Pt(211), however, the situation becomes slightly different. As the H_2/C_3H_8 ratio rises, the forward reaction rate of r_9 is initially promoted more dramatically than the reverse reaction rate (see Figure 9b) and, consequently, less propane is converted to the adsorbed propylene via r_9. When the H_2/C_3H_8 ratio is higher than 2, the forward reaction becomes dominant, meaning that propylene is consumed rather than being produced and becomes a primary product that reacts further to form by-products. In addition, the increase in the H_2/C_3H_8 ratio has a more pronounced effect on the acceleration of the forward reaction of r_{50} than on that of the reverse, giving rise to an increased contribution from CH_3CCH_f to the cracking reaction. Interestingly, at low H_2/C_3H_8 ratios less than 1.33, the cracking of the C3 species tends to start from CH_3CCH_s via r_{49}, which arises from the large increase in the Gibbs free energy barrier for the dehydrogenation of CH_3CCH_s due to the presence of the adsorbate-adsorbate interactions. Finally, although the mechanism for the side reaction may change slightly with the H_2/C_3H_8 ratio, the dominant reaction pathway for propylene production over Pt(211) still follows the non-reverse Horiuti-Polanyi mechanism, as reflected in the large value of the percentage of the reaction flux for r_{11}.

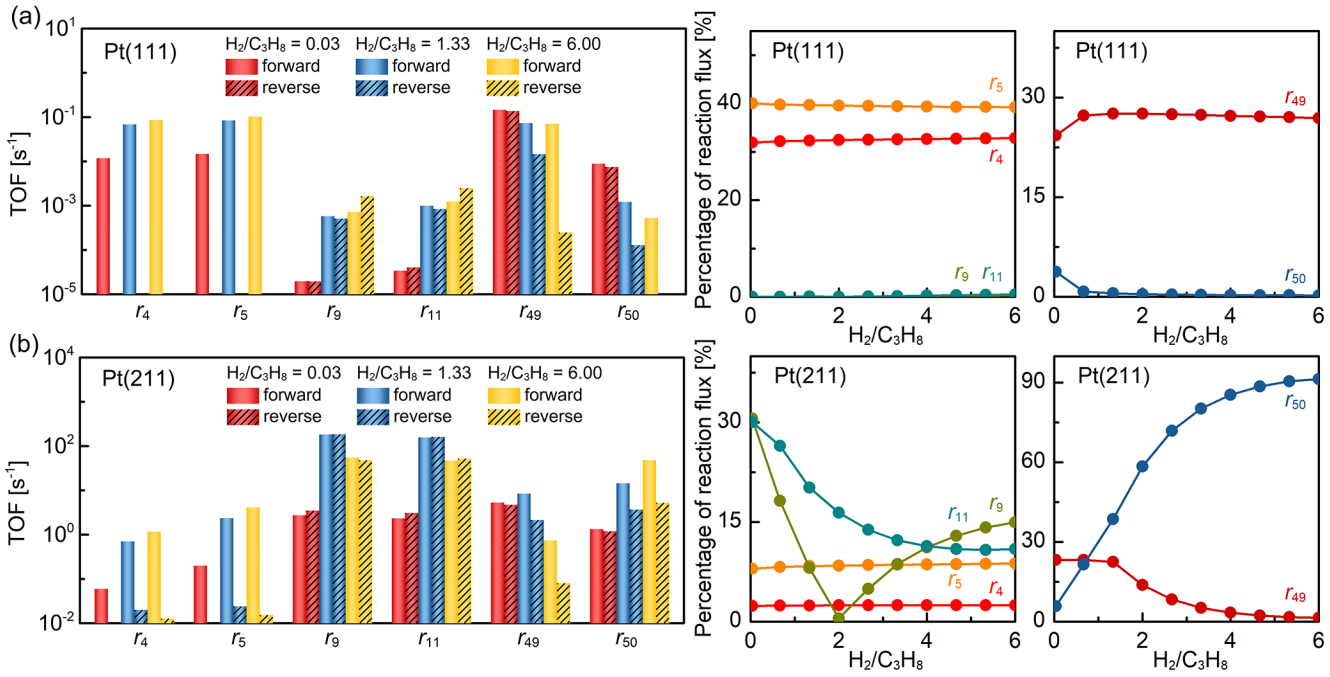

Figure 9. Forward and reverse reaction rates of elementary steps obtained from microkinetic model with adsorbate-adsorbate interactions at 723.15 K, 0.03 bar of propane, and H_2/C_3H_8 ratios of 0.03, 1.33, and 6.00, and percentage of the reaction flux for elementary steps as a function of the H_2/C_3H_8 ratio over (a) Pt(111) and (b) Pt(211).

3.5.2. Sensitivity Analysis

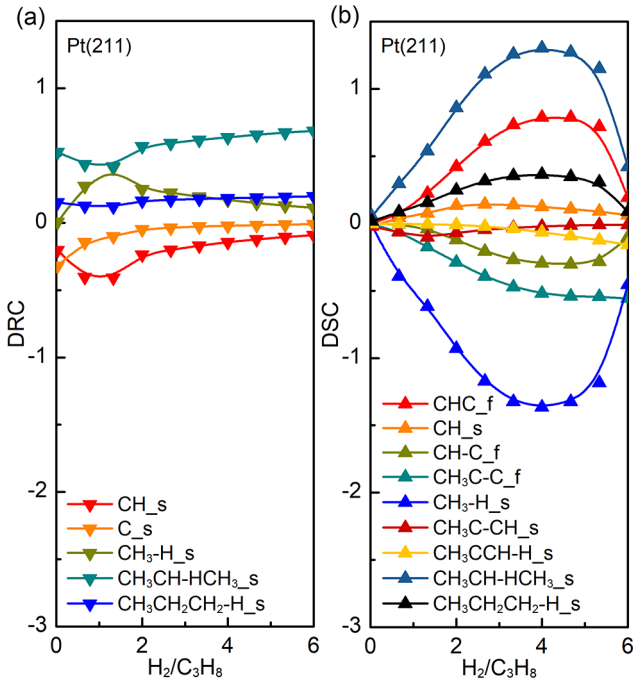

Figure 10. Plots of (a) degree of rate control (DRC) for propane consumption and (b) degree of selectivity control (DSC) for propylene production obtained from microkinetic analysis with adsorbate-adsorbate interactions over Pt(211) as a function of the H_2/C_3H_8 ratio at 723.15 K and 0.03 bar of propane.

To examine more closely the key factors that influence the catalytic activity and selectivity of the more active Pt(211) surface, it is advantageous to conduct sensitivity analysis by calculating the degree of rate control (DRC) for propane consumption and the degree of selectivity control (DSC) for propylene production. These two quantities have been widely used in the investigation of complex reactions taking place by mechanisms that involve several elementary steps.[58, 63, 66]

In this work, the DRC that is originally proposed by Stegelmann et al.[67-68] is calculated as the relative change of the propane consumption rate in response to the variation of the Gibbs free energy of reaction intermediate (or transition state) i while keeping the Gibbs free energies of all other intermediates and transition states fixed:

$$DRC(i) = \frac{1}{TOF_{\text{propane}}}\left[\frac{dTOF_{\text{propane}}}{d\left(-G_i / k_{\text{B}}T\right)}\right]_{G_{n\neq i}} = \frac{d\left(lnTOF_{\text{propane}}\right)}{d\left(-G_i / k_{\text{B}}T\right)_{G_{n\neq i}}} \quad (9)$$

which provide a measure of the degree to which the TOF_{propane} would depend upon the Gibbs free energy of that species. In much the same way, the DSC for the catalyst selectivity ($S_{\text{propylene}}$) toward propylene production can be written as

$$DSC(i) = \frac{1}{S_{\text{propylene}}}\left[\frac{dS_{\text{propylene}}}{d\left(-G_i / k_B T\right)}\right]_{G_{n\neq i}} = \frac{d\left(lnS_{\text{propylene}}\right)}{d\left(-G_i / k_B T\right)_{G_{n\neq i}}} \quad (10)$$

Under these definitions, the larger the magnitude of DRC (or DSC), the more greatly would the energy level of that

species influence the TOF_{propane} (or $S_{\text{propylene}}$). Moreover, a positive DRC (or DSC) indicates that decreasing the Gibbs free energy of that species may increase the TOF_{propane} (or $S_{\text{propylene}}$) while a negative value implies the opposite.

It can be seen from Figure 10a that, under the reaction conditions of interest, the Gibbs free energy of the transition state for the dehydrogenation of propane to 2-propyl (CH_3CH-HCH_3_s) have the largest absolute value of DRC, suggesting that the rate of propane consumption is most sensitive to the Gibbs free energy of CH_3CH-HCH_3_s. The finding that the first dehydrogenation step is the rate-limiting step for the overall reaction is in remarkably good agreement with experimental observations.[12] The positive value of DRC for CH_3CH-HCH_3_s indicates that the TOF_{propane} would decrease if the Gibbs free energy of CH_3CH-HCH_3_s become more negative. Nevertheless, some other species would also play a role in controlling the overall rate, especially at low H_2/C_3H_8 ratios. For instance, the DRCs for CH_3CH-HCH_3_s, CH_s, and C_s are calculated to be 0.525, -0.202, and -0.319, respectively, taking comparable values at the H_2/C_3H_8 ratio of 0.33. Thus, the catalytic activity also depends upon the stability of CH_s and C_s, and the negative DRC values signify that the propane consumption rate may rise if CH_s and C_s could be destabilized. This relationship makes sense because CH_s and C_s are the abundant reaction intermediates on Pt(211) and tend to block free sites that are required for propane activation.

Figure 10b depicts the calculated DSCs as a function of the H_2/C_3H_8 ratio. From the figure, one can see that the $S_{\text{propylene}}$ over Pt(211) is most affected by the Gibbs free energies of the transition state for the activation of C-H bonds in propane (CH_3CH-HCH_3_s) and methane (CH_3-H_s). The DSCs for CH_3CH-HCH_3_s and CH_3-H_s have opposite signs, indicating that the lowering of the activation energies for PDH and methane formation has a positive and negative effect on the catalyst selectivity, respectively. Although the activation of propane would also give rise to side products in addition to propylene, the acceleration of this step apparently plays a beneficial role in the production of propylene. In addition, it is interesting to find that the $S_{\text{propylene}}$ can be increased if CHC_f is bound more tightly to the surface. The reasoning behind this remark is that CHC_f is the most abundant reaction intermediate at the "f" site and the decreased coverage of free "f" sites has a positive effect on the catalyst selectivity, which is consistent with the finding in Section 3.4 that the growth in the coverage of *_f accelerates the rate of the deep dehydrogenation and cracking reactions.

4. CONCLUSION

In this contribution, a detailed DFT-assisted microkinetic analysis that includes adsorbate-adsorbate interactions has been carried out to interpret the kinetics of PDH over Pt catalysts. The experimental results show that the rate for propane consumption increases as the H_2/C_3H_8 ratio goes up, but the rate of production of propylene first increases and then goes down. These characteristic features are then used to validate and confirm the theoretically determined kinetics. It is found that the patterns of the dependence of the $TOF_{propane}$ and $TOF_{propylene}$ can be well reproduced and the optimum H_2/C_3H_8 ratio of around 1.30 can be predicted with reasonable accuracy after the lateral interactions are considered in the microkinetic model.

The activity of Pt(211) is orders of magnitude greater than that of Pt(111), and its selectivity toward propylene decreases steadily with the H_2/C_3H_8 ratio, bearing close resemblance to the experiment. Thus, the under-coordinated Pt atoms cannot be completely deactivated under realistic reaction conditions and are expected to dominate the catalytic behavior of the prepared catalyst, even although terraces have a much higher mole fraction on the catalyst surface. Through the flux analysis, we find that the conversion from propane to propylene on Pt(111) occurs by the generally accepted reverse Horiuti-Polanyi mechanism, and the formation of propylene and by-products proceeds essentially by way of two parallel reactions starting from CH_3CHCH_3. On Pt(211), however, an unexpected reaction pathway is proposed to dominate the kinetics, which consists of three dehydrogenation steps that have two β-H and one α-H atoms removed from propane, followed by the hydrogenation of CH_3CCH_2, and at this species the deep dehydrogenation reaction competes with the production of propylene. The subsequent sensitivity analysis shows that the first dehydrogenation step in propane controls the rate of the overall reaction and the selectivity toward propylene is determined largely by the competition between propane activation and methane formation.

The formulation of the non-reverse Horiuti-Polanyi mechanism here is expected to be of great and general importance for a molecular-level view of the pathway from alkane to alkene, which would in turn boost the computational design of metal and alloy catalysts for the light alkane dehydrogenation reactions.

ASSOCIATED CONTENT

Supporting Information: Experimental turnover frequency (TOF) calculation, reaction network for propane dehydrogenation (PDH), optimized geometries of adsorbed species and activated complexes involved in PDH over Pt(111) and Pt(211), experimental results, multi-site microkinetic model of PDH, relationship between Pt cluster size and the ratio of Pt(111) and Pt(211), surface coverages over Pt(111) and Pt(211) obtained from the microkinetic

model without adsorbate-adsorbate interactions, adsorbate-adsorbate interaction model over Pt(111) and Pt(211), surface coverages over Pt(111) and Pt(211) obtained from the microkinetic model with adsorbate-adsorbate interactions, the role of the hydrogen, microkinetic analysis without adsorbate-adsorbate interactions, flux analysis.

AUTHOR INFORMATION

Corresponding Author

* Email: yanzhu@ecust.edu.cn (Yi-An Zhu)

Author Contributions

# These authors contributed equally.

Notes

The authors declare no competing financial interest.

ACKNOWLEDGMENT

This work is supported by the Natural Science Foundation of China (91645122, 22073027, and U1663221), the Natural Science Foundation of Shanghai (No. 20ZR1415800), the National Key Research and Development Program of China (2018YFB0604700), and the Fundamental Research Funds for the Central Universities (222201718003). The computational time provided by the Notur project is highly acknowledged.

REFERENCES

(1) Sattler, J. J.; Ruiz-Martinez, J.; Santillan-Jimenez, E.; Weckhuysen, B. M., Catalytic Dehydrogenation of Light Alkanes on Metals and Metal Oxides. *Chem. Rev.* **2014,** *114*, 10613-10653.

(2) Christophe, C.; Florian, A.; Wing, C. K.; P., C. M.; F., D. M.; Alexey, F.; B., M. I.; Victor, M.; Margherita, P.; Keith, S.; Keishi, Y.; A., Z. P., Bridging the Gap between Industrial and Well-Defined Supported Catalysts. *Angew. Chem. Int. Ed.* **2018,** *57*, 6398-6440.

(3) Bruijnincx, P. C. A.; Weckhuysen, B. M., Shale Gas Revolution: An Opportunity for the Production of Biobased Chemicals? *Angew. Chem. Int. Ed.* **2013,** *52*, 11980-11987.

(4) McFarland, E., Unconventional Chemistry for Unconventional Natural Gas. *Science* **2012,** *338*, 340-342.

(5) National Academies of Sciences, E., Medicine, *The Changing Landscape of Hydrocarbon Feedstocks for Chemical Production: Implications for Catalysis: Proceedings of a Workshop*. National Academies Press: 2016.

(6) Heinritz-Adrian, M.; Wenzel, S.; Youssef, F., Advanced Propane Dehydrogenation. *Petroleum Technology Quarterly* **2008,** *13*, 83-92.

(7) Im, J.; Choi, M., Physicochemical Stabilization of Pt Against Sintering for a Dehydrogenation Catalyst with High Activity, Selectivity, and Durability. *ACS Catal.* **2016,** *6*, 2819-2826.

(8) Zhu, Y.; An, Z.; Song, H.; Xiang, X.; Yan, W.; He, J., Lattice-Confined Sn (IV/II) Stabilizing Raft-Like Pt Clusters: High Selectivity and Durability in Propane Dehydrogenation. *ACS Catal.* **2017,** *7*, 6973-6978.

(9) Yang, M.-L.; Zhu, Y.-A.; Fan, C.; Sui, Z.-J.; Chen, D.; Zhou, X.-G., Density Functional Study of the Chemisorption of C_1, C_2 and C_3 intermediates in Propane Dissociation on Pt(111). *J. Mol. Catal. A: Chem.* **2010,** *321*, 42-49.

(10) Bariås, O. A.; Holmen, A.; Blekkan, E. A., Propane Dehydrogenation over Supported Pt and Pt-Sn Catalysts: Catalyst Preparation, Characterization, and Activity Measurements. *J. Catal.* **1996,** *158*, 1-12.

(11) Horiuti, I.; Polanyi, M., Exchange Reactions of Hydrogen on Metallic Catalysts. *Trans. Faraday Soc.* **1934,** *30*, 1164-1172.

(12) Zhu, J.; Yang, M.-L.; Yu, Y.; Zhu, Y.-A.; Sui, Z. J.; Zhou, X.; Holmen, A.; Chen, D., Size-Dependent Reaction Mechanism and Kinetics for Propane Dehydrogenation over Pt Catalyst. *ACS Catal.* **2015,** *5*, 6310-6319.

(13) Zha, S.; Sun, G.; Wu, T.; Zhao, J.; Zhao, Z.-J.; Gong, J., Identification of Pt-based Catalysts for Propane Dehydrogenation via a Probability Analysis. *Chem. Sci.* **2018,** *9*, 3925-3931.

(14) Cai, W.; Mu, R.; Zha, S.; Sun, G.; Chen, S.; Zhao, Z.-J.; Li, H.; Tian, H.; Tang, Y.; Tao, F.; Zeng, L.; Gong, J., Subsurface Catalysis-Mediated Selectivity of Dehydrogenation Reaction. *Sci. Adv.* **2018,** *4*, eaar5418.

(15) Wang, T.; Jiang, F.; Liu, G.; Zeng, L.; Zhao, Z. j.; Gong, J., Effects of Ga Doping on Pt/CeO_2-Al_2O_3 Catalysts for Propane Dehydrogenation. *AlChE J.* **2016,** *62*, 4365-4376.

(16) Zhao, Z.-J.; Chiu, C.-c.; Gong, J., Molecular Understandings on the Activation of Light Hydrocarbons over Heterogeneous Catalysts. *Chem. Sci.* **2015,** *6*, 4403-4425.

(17) Yang, M.-L.; Zhu, Y.-A.; Fan, C.; Sui, Z.-J.; Chen, D.; Zhou, X.-G., DFT Study of Propane Dehydrogenation on Pt Catalyst: Effects of Step Sites. *Phys. Chem. Chem. Phys.* **2011,** *13*, 3257-3267.

(18) Xiao, L.; Ma, F.; Zhu, Y.-A.; Sui, Z.-J.; Zhou, J.-H.; Zhou, X.-G.; Chen, D.; Yuan, W.-K., Improved Selectivity and Coke Resistance of Core-Shell Alloy Catalysts for Propane Dehydrogenation from First Principles and Microkinetic Analysis. *Chem. Eng. J.* **2019,** *377*, 120049.

(19) Yang, M.-L.; Fan, C.; Zhu, Y.-A.; Sui, Z.-J.; Zhou, X.-G.; Chen, D., Selective Oxidation of Hydrogen in the Presence of Propylene over Pt-Based Core-Shell Nanocatalysts. *J. Phys. Chem. C* **2015,** *119*, 21386-21394.

(20) Lian, Z.; Ali, S.; Liu, T.; Si, C.; Li, B.; Su, D. S., Revealing the Janus Character of the Coke Precursor in the Propane Direct Dehydrogenation on Pt Catalysts from a kMC Simulation. *ACS Catal.* **2018,** *8*, 4694-4704.

(21) Saerens, S.; Sabbe, M. K.; Galvita, V. V.; Redekop, E. A.; Reyniers, M.-F.; Marin, G. B., The Positive Role of Hydrogen on the Dehydrogenation of Propane on Pt(111). *ACS Catal.* **2017,** *7*, 7495-7508.

(22) Larsson, M.; Hultén, M.; Blekkan, E. A.; Andersson, B., The Effect of Reaction Conditions and Time on Stream on the Coke Formed during Propane Dehydrogenation. *J. Catal.* **1996,** *164*, 44-53.

(23) Kumar, M. S.; Chen, D.; Walmsley, J. C.; Holmen, A., Dehydrogenation of Propane over Pt-SBA-15: Effect of Pt Particle Size. *Catal. Commun.* **2008,** *9*, 747-750.

(24) Redekop, E. A.; Saerens, S.; Galvita, V. V.; González, I. P.; Sabbe, M.; Bliznuk, V.; Reyniers, M.-F.; Marin, G. B., Early

Stages in the Formation and Burning of Graphene on a Pt/Mg(Al)Ox Dehydrogenation Catalyst: A temperature- and Time-Resolved Study. *J. Catal.* **2016,** *344*, 482-495.

(25) Viñes, F.; Lykhach, Y.; Staudt, T.; Lorenz, M. P. A.; Papp, C.; Steinrück, H.-P.; Libuda, J.; Neyman, K. M.; Görling, A., Methane Activation by Platinum: Critical Role of Edge and Corner Sites of Metal Nanoparticles. *Chem.-Eur. J.* **2010,** *16*, 6530-6539.

(26) Peng, Z.; Somodi, F.; Helveg, S.; Kisielowski, C.; Specht, P.; Bell, A. T., High-Resolution in situ and ex situ TEM Studies on Graphene Formation and Growth on Pt Nanoparticles. *J. Catal.* **2012,** *286*, 22-29.

(27) Liu, Z.-P.; Hu, P., General Rules for Predicting Where a Catalytic Reaction Should Occur on Metal Surfaces: A Density Functional Theory Study of C-H and C-O Bond Breaking/Making on Flat, Stepped, and Kinked Metal Surfaces. *J. Am. Chem. Soc.* **2003,** *125*, 1958-1967.

(28) Sun, X.; Han, P.; Li, B.; Zhao, Z., Tunable Catalytic Performance of Single Pt Atom on the Doped Graphene in Direct Dehydrogenation of Propane by Rational Doping: A Density Functional Theory Study. *J. Phys. Chem. C* **2018,** *122*, 1570-1576.

(29) Wei, H.; Liu, X.; Wang, A.; Zhang, L.; Qiao, B.; Yang, X.; Huang, Y.; Miao, S.; Liu, J.; Zhang, T., FeOx-Supported Platinum Single-Atom and Pseudo-Single-Atom Catalysts for Chemoselective Hydrogenation of Functionalized Nitroarenes. *Nat. Commun.* **2014,** *5*, 5634.

(30) Wei, H.; Ren, Y.; Wang, A.; Liu, X.; Liu, X.; Zhang, L.; Miao, S.; Li, L.; Liu, J.; Wang, J.; Wang, G.; Su, D.; Zhang, T., Remarkable Effect of Alkalis on the Chemoselective Hydrogenation of Functionalized Nitroarenes over High-Loading Pt/FeO_x Catalysts. *Chem. Sci.* **2017,** *8*, 5126-5131.

(31) Lausche, A. C.; Medford, A. J.; Khan, T. S.; Xu, Y.; Bligaard, T.; Abild-Pedersen, F.; Nørskov, J. K.; Studt, F., On the Effect of Coverage-Dependent Adsorbate-Adsorbate Interactions for CO Methanation on Transition Metal Surfaces. *J. Catal.* **2013,** *307*, 275-282.

(32) Grabow, L. C.; Hvolbæk, B.; Nørskov, J. K., Understanding Trends in Catalytic Activity: The Effect of Adsorbate–Adsorbate Interactions for CO Oxidation over Transition Metals. *Top. Catal.* **2010,** *53*, 298-310.

(33) Zhou, M.; Liu, B., First-Principles Investigation of Adsorbate–Adsorbate Interactions on Ni(111), Ni(211), and Ni(100) Surfaces. *Ind. Eng. Chem. Res.* **2017,** *56*, 5813-5820.

(34) Kresse, G.; Hafner, J., Ab Initio Molecular Dynamics for Liquid Metals. *Phys. Rev. B* **1993,** *47*, 558-561.

(35) Kresse, G.; Furthmüller, J., Efficiency of Ab-initio Total Energy Calculations for Metals and Semiconductors Using a Plane-Wave Basis Set. *Comp. Mater. Sci.* **1996,** *6*, 15-50.

(36) Kresse, G.; Furthmüller, J., Efficient Iterative Schemes for Ab initio Total-Energy Calculations Using a Plane-Wave Basis Set. *Phys. Rev. B* **1996,** *54*, 11169-11186.

(37) Blöchl, P. E., Projector Augmented-Wave Method. *Phys. Rev. B* **1994,** *50*, 17953-17979.

(38) Monkhorst, H. J.; Pack, J. D., Special Points for Brillouin-Zone Integrations. *Phys. Rev. B* **1976,** *13*, 5188-5192.

(39) Methfessel, M.; Paxton, A. T., High-Precision Sampling for Brillouin-Zone Integration in Metals. *Phys. Rev. B* **1989,** *40*, 3616-3621.

(40) Wellendorff, J.; Lundgaard, K. T.; Møgelhøj, A.; Petzold, V.; Landis, D. D.; Nørskov, J. K.; Bligaard, T.; Jacobsen, K. W., Density Functionals for Surface Science: Exchange-Correlation Model Development with Bayesian Error Estimation. *Phys. Rev. B* **2012,** *85*, 235149.

(41) Gautier, S.; Steinmann, S. N.; Michel, C.; Fleurat-Lessard, P.; Sautet, P., Molecular Adsorption at Pt (111). How Accurate are DFT Functionals? *Phys. Chem. Chem. Phys.* **2015,** *17*, 28921-28930.

(42) Sheppard, D.; Terrell, R.; Henkelman, G., Optimization Methods for Finding Minimum Energy Paths. *J. Chem. Phys.* **2008,** *128*, 134106.

(43) Henkelman, G.; Jónsson, H., A Dimer Method for Finding Saddle Points on High Dimensional Potential Surfaces Using only First Derivatives. *J. Chem. Phys.* **1999,** *111*, 7010-7022.

(44) Hansen, M. H.; Nørskov, J. K.; Bligaard, T., First Principles Micro-Kinetic Model of Catalytic Non-Oxidative Dehydrogenation of Ethane over Close-Packed Metallic Facets. *J. Catal.* **2019,** *374*, 161-170.

(45) Cao, A.; Schumann, J.; Wang, T.; Zhang, L.; Xiao, J.; Bothra, P.; Liu, Y.; Abild-Pedersen, F.; Nørskov, J. K., Mechanistic Insights into the Synthesis of Higher Alcohols from Syngas on CuCo Alloys. *ACS Catal.* **2018,** *8*, 10148-10155.

(46) Medford, A. J.; Shi, C.; Hoffmann, M. J.; Lausche, A. C.; Fitzgibbon, S. R.; Bligaard, T.; Nørskov, J. K., CatMAP: A Software Package for Descriptor-Based Microkinetic Mapping of Catalytic Trends. *Catal. Lett.* **2015,** *145*, 794-807.

(47) Cramer, C. J., *Essentials of Computational Chemistry: Theories and Models*. J. Wiley & Sons, Ltd: 2004.

(48) Bahn, S. R.; Jacobsen, K. W., An Object-Oriented Scripting Interface to a Legacy Electronic Structure Code. *Comput. Sci. Eng.* **2002,** *4*, 56-66.

(49) Cortright, R. D.; Dumesic, J. A., Kinetics of Heterogeneous Catalytic Reactions: Analysis of Reaction Schemes. *Adv. Catal.* **2001,** *46*, 161-264.

(50) Shan, Y.-L.; Zhu, Y.-A.; Sui, Z.-J.; Chen, D.; Zhou, X.-G., Insights into the Effects of Steam on Propane Dehydrogenation over Pt/Al_2O_3 Catalyst. *Catal. Sci. Technol.* **2015,** *5*, 3991-4000.

(51) Yang, M.-L.; Zhu, J.; Zhu, Y.-A.; Sui, Z.-J.; Yu, Y.-D.; Zhou, X.-G.; Chen, D., Tuning Selectivity and Stability in Propane Dehydrogenation by Shaping Pt Particles: A Combined Experimental and DFT Study. *J. Mol. Catal. A: Chem.* **2014,** *395*, 329-336.

(52) Valcárcel, A.; Ricart, J. M.; Clotet, A.; Illas, F.; Markovits, A.; Minot, C., Theoretical Study of Dehydrogenation and Isomerisation Reactions of Propylene on Pt(111). *J. Catal.* **2006,** *241*, 115-122.

(53) Galvita, V.; Siddiqi, G.; Sun, P.; Bell, A. T., Ethane Dehydrogenation on Pt/Mg(Al)O and PtSn/Mg(Al)O Catalysts. *J. Catal.* **2010,** *271*, 209-219.

(54) Siddiqi, G.; Sun, P.; Galvita, V.; Bell, A. T., Catalyst Performance of Novel Pt/Mg(Ga)(Al)O Catalysts for Alkane Dehydrogenation. *J. Catal.* **2010,** *274*, 200-206.

(55) Wu, J.; Sharada, S. M.; Ho, C.; Hauser, A. W.; Head-Gordon, M.; Bell, A. T., Ethane and Propane

Dehydrogenation over PtIr/Mg(Al)O. *Appl. Catal. A: Gen.* **2015,** *506*, 25-32.

(56) Wu, J.; Peng, Z.; Sun, P.; Bell, A. T., n-Butane Dehydrogenation over Pt/Mg(In)(Al)O. *Appl. Catal. A: Gen.* **2014,** *470*, 208-214.

(57) Dumesic, J. A., *The Microkinetics of Heterogeneous Catalysis*. An American Chemical Society Publication: 1993.

(58) Wu, P.; Yang, B., Significance of Surface Formate Coverage on the Reaction Kinetics of Methanol Synthesis from CO_2 Hydrogenation over Cu. *ACS Catal.* **2017,** *7*, 7187-7195.

(59) Ligthart, D. A. J. M.; van Santen, R. A.; Hensen, E. J. M., Influence of Particle Size on the Activity and Stability in Steam Methane Reforming of Supported Rh Nanoparticles. *J. Catal.* **2011,** *280*, 206-220.

(60) Van Hardeveld, R.; Hartog, F., The Statistics of Surface Atoms and Surface Sites on Metal Crystals. *Surf. Sci.* **1969,** *15*, 189-230.

(61) Nørskov, J. K.; Bligaard, T.; Rossmeisl, J.; Christensen, C. H., Towards the Computational Design of Solid Catalysts. *Nature Chem.* **2009,** *1*, 37-46.

(62) Yao, Z.; Guo, C.; Mao, Y.; Hu, P., Quantitative Determination of C-C Coupling Mechanisms and Detailed Analyses on the Activity and Selectivity for Fischer-Tropsch Synthesis on Co(0001): Microkinetic Modeling with Coverage Effects. *ACS Catal.* **2019,** *9*, 5957-5973.

(63) Huš, M.; Hellman, A., Ethylene Epoxidation on Ag(100), Ag(110), and Ag(111): A Joint Ab Initio and Kinetic Monte Carlo Study and Comparison with Experiments. *ACS Catal.* **2019,** *9*, 1183-1196.

(64) Yang, N.; Medford, A. J.; Liu, X.; Studt, F.; Bligaard, T.; Bent, S. F.; Nørskov, J. K., Intrinsic Selectivity and Structure Sensitivity of Rhodium Catalysts for C_{2+} Oxygenate Production. *J. Am. Chem. Soc.* **2016,** *138*, 3705-3714.

(65) Nørskov, J. K.; Studt, F.; Abild-Pedersen, F.; Bligaard, T., *Fundamental Concepts in Heterogeneous Catalysis*. John Wiley & Sons: 2014.

(66) Nørskov, J. K.; Bligaard, T.; Kleis, J., Rate Control and Reaction Engineering. *Science* **2009,** *324*, 1655-1656.

(67) Stegelmann, C.; Andreasen, A.; Campbell, C. T., Degree of Rate Control: How Much the Energies of Intermediates and Transition States Control Rates. *J. Am. Chem. Soc.* **2009,** *131*, 8077-8082.

(68) Campbell, C. T., The Degree of Rate Control: A Powerful Tool for Catalysis Research. *ACS Catal.* **2017,** *7*, 2770-2779.

TOC Graphic

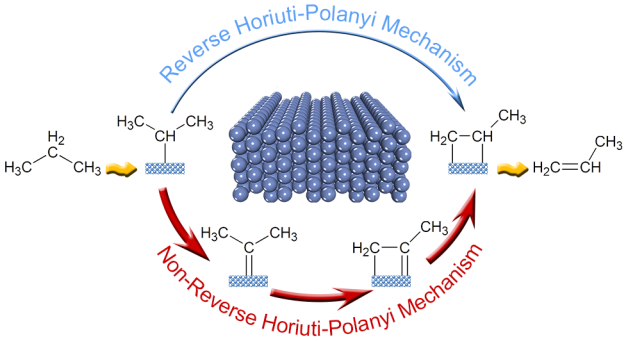
Reverse Horiuti-Polanyi Mechanism
Non-Reverse Horiuti-Polanyi Mechanism